Inorganic Chemistry

Article

pubs.acs.org/IC

Sensitizer-Catalyst Assemblies for Water Oxidation

Lei Wang,[†,⊥] Mohammad Mirmohades,[‡,⊥] Allison Brown,[‡] Lele Duan,[†] Fusheng Li,[†] Quentin Daniel,[†] Reiner Lomoth,[‡] Licheng Sun,[†,§] and Leif Hammarström*[,‡]

[†]Department of Chemistry, School of Chemical Science and Engineering, KTH Royal Institute of Technology, 10044 Stockholm, Sweden

[‡]Photochemistry and Molecular Science, Department of Chemistry—Ångström Laboratory, Uppsala University, Box 523, SE-751 20 Uppsala, Sweden

[§]State Key Lab of Fine Chemicals, DUT-KTH Joint Education and Research Center on Molecular Devices, Dalian University of Technology (DUT), 116024 Dalian, China

Supporting Information

ABSTRACT: Two molecular assemblies with one Ru(II)-polypyridine photosensitizer covalently linked to one Ru(II)(bda)L_2 catalyst (**1**) (bda = 2,2′-bipyridine-6,6′-dicarboxylate) and two photosensitizers covalently linked to one catalyst (**2**) have been prepared using a simple C−C bond as the linkage. In the presence of sodium persulfate as a sacrificial electron acceptor, both of them show high activity for catalytic water oxidation driven by visible light, with a turnover number up to 200 for **2**. The linked photocatalysts show a lower initial yield for light driven oxygen evolution but a much better photostability compared to the three component system with separate sensitizer, catalyst and acceptor, leading to a much greater turnover number. Photocatalytic experiments and time-resolved spectroscopy were carried out to probe the mechanism of this catalysis. The linked catalyst in its Ru(II) state rapidly quenches the sensitizer, predominantly by energy transfer. However, a higher stability under photocatalytic condition is shown for the linked sensitizer compared to the three component system, which is attributed to kinetic stabilization by rapid photosensitizer regeneration. Strategies for employment of the sensitizer-catalyst molecules in more efficient photocatalytic systems are discussed.

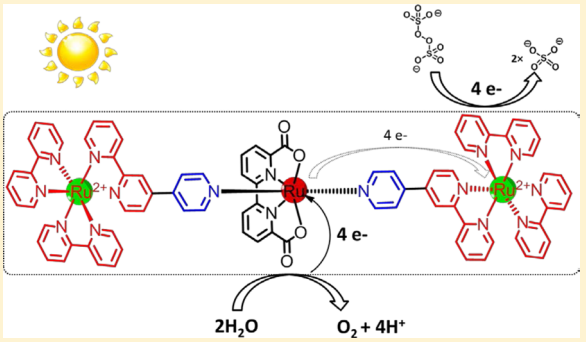

INTRODUCTION

Splitting water efficiently by artificial photosynthesis to generate hydrogen and oxygen driven by sunlight is one of the most attractive pursuits in the field of solar energy conversion.[1] There are two essential half reactions in artificial photosynthesis:[2] water oxidation to molecular oxygen

$$2H_2O \rightarrow O_2 + 4H^+ + 4e^-$$

and the reduction of substrate to a fuel, e.g.

$$4H^+ + 4e^- \rightarrow 2H_2 \text{ or } CO_2 + 2H^+ + 2e^- \rightarrow CO + H_2O$$

The first half reaction has long been considered to be the bottleneck because four consecutive proton-coupled electron transfer steps are needed for the production of one oxygen molecule. Therefore, the development of efficient and robust water oxidation photocatalysts is of great importance.

So far, there have been many water oxidation catalysts (WOCs) developed: most of these are Ru complexes[2−12] while others include complexes of Ir,[13−15] Co,[16−22] Fe,[23,24] and Cu.[25,26] However, very few effective photocatalysts are documented because (i) most molecular water oxidation catalysts possess high onset potentials for water oxidation which are close to or even higher than the oxidation potential of the commonly used photosensitizer $[Ru(bpy)_3]^{2+}$, and (ii) the synthetic and purification work of the sensitizer-catalyst dyad assembly is complicated. Therefore, a three-component system in homogeneous solution is usually employed to evaluate the light-driven water oxidation activity of molecular water oxidation catalysts.[16,27−30] The system is composed of (i) a photosensitizer that can be excited to a long-lived (>50 ns) excited state by visible light, (ii) a sacrificial electron acceptor to oxidatively quench the excited photosensitizer, and (iii) a WOC that could be oxidized by the oxidized photosensitizer and eventually oxidize water. In such a system, the electron transfer from the catalyst to the photosensitizer is limited by diffusional encounter. To overcome diffusion-limited electron transfer, one way is to link these two components together via covalent bonds to form an all-in-one assembled photocatalyst (Scheme 1). This may increase the transfer rate of oxidizing equivalents to the catalyst; while this step is not necessarily rate limiting for a photocatalytic process it ensures a rapid regeneration of the highly oxidizing sensitizer that may lower the risk of sensitizer degradation in side reactions.

Received: December 5, 2014
Published: February 20, 2015

DOI: 10.1021/ic502915r
Inorg. Chem. 2015, 54, 2742−2751

Scheme 1. General Concept of Photocatalyst for Water Oxidation

Recently, Meyer,[31] Thummel,[32] Wasielewski,[33] and our group[34,35] have reported some supramolecular photocatalysts combining WOCs and photosensitizers together in order to realize highly efficient water-oxidation photocatalysts in homogeneous system. It turns out that the catalysis assemblies are often more efficient than the corresponding three-component system under the same catalytic conditions.

For our previously studied systems, see Scheme 2, structures **a** and **b1**−**3**, it is not yet clear what factors control the observed differences in catalytic activities. Although **b3** shows higher turnovers than **b1** under the same conditions, the initial reaction rate of **b3** is much lower than that of **b1**. On the other hand, when comparing Meyer's[31] and Thummel's[32] photocatalysts, we note that the major structural difference is the bridging ligands, and the results show that the system with the shorter bridge gives the higher photocatalytic activity. To further study this type of assemblies, with short bridging ligands by the means of electron transfer kinetics, we herein synthesized two supramolecular photocatalysts (**1** and **2** in Scheme 2) by connecting the catalyst to $[Ru(bpy)_3]^{2+}$ motifs via a short C−C bond, based on the recently reported Ru-bda water oxidation catalysts $[Ru(bda)L_2]$ (H_2bda = 2,2′-bipyridine-6,6′-dicarboxylic acid; L = N-containing aromatic ligands) with high activities and low overpotentials.[6,8] The electrochemical, photophysical, and light-driven water oxidation properties of **1** and **2** were investigated.

The comparison between complexes **1** and **2** could provide more insights into such assemblies, such as the effect of the quantity of $[Ru(bpy)_3]^{2+}$ moiety on the catalysis efficiency and stability. The short bridge between sensitizer and catalyst could enhance the intramolecular electron transfer rate in principle for both directions: from sensitizer to catalyst and vice versa.

EXPERIMENTAL SECTION

Materials and Synthesis. All chemicals and solvents, if not stated otherwise, were purchased from Sigma-Aldrich without further purification. 2,2′-Bipyridine-6,6′-dicarboxylic (bda H_2) was purchased from Jinan Henghua Science & Technology Co. Ltd.; *cis*-$[Ru(dmso)_4Cl_2]$,[36] 2,2′-bipyridyl *N*-oxide (**a**),[37] 4-nitro-2,2′-bipyridine *N*-oxide (**b**),[37] 4-bromo-2,2′-bipyridine-*N*-oxide (**c**),[38] 4-bromo-2,2′-bipyridine (**d**),[38] and *cis*-$[Ru(bpy)_2Cl_2]$ (**f**)[39] were synthesized following literature methods. The ^1H NMR spectra were recorded on a 500 MHz Bruker Avance NMR spectrometer with TMS as internal standard. Mass spectra were performed by electrospray ionization (ESI) on an HP 1100 MSD instrument.

*2,2′:4′,4″-Terpyridine (bpyp) (**e**).* 4-Bromo-2,2′-bipyridine (**d**) (1.17 g, 5.0 mmol), 4-pyridinylboronic acid (0.8 g, 6.5 mmol), $[Pd(dppf)Cl_2]$ [dppf = 1,1′-bis(diphenylphosphino)ferrocene] (450 mg, 16 mol %), Cs_2CO_3 (500 mg), and 20 mL CH_3OH/toluene (1:1) were added to a Schlenk-type flask (100 mL) equipped with a rubber septum. The solution was degassed by argon. The mixture was then stirred at 100 °C for 24 h. The reaction was stopped, the reaction mixture was cooled to room temperature, and the solvent was removed by evaporation at elevated temperature. The crude product was added to a mixture of an aqueous 0.5 N NaOH solutions (30 mL) and ethyl acetate (30 mL). The aqueous layer was washed with ethyl acetate (30 mL × 3) to remove the unreacted boronic acid. The combined organic layers were washed with an aqueous 0.5 N NaOH solution (40 mL × 3). Then, the organic layer was dried in vacuum and purified by column chromatography on silica gel using DCM/CH_3OH (40:1) as eluents. **e** was obtained as colorless powder (yield: 29%, 0.33 g). ^1H NMR (500 MHz, $CDCl_3$): δ = 8.80 (d, J = 5.0 Hz, 1 H), 8.76 (m, 2 H), 8.71 (s, 2 H), 8.41 (d, J = 8.0 Hz, 1 H), 7.86 (m, 1 H), 7.76 (m, 2 H), 7.56 (m, 1 H), 7.36 (m, 1 H). ES-MS$^+$: m/z^+ = 234.13 (M + H^+), calcd 234.1026.

*[Ru(bda)(dmso)$_2$] (**g**).* A mixture of 2,2′-bipyridine-6,6′-dicarboxylic acid (244 mg, 1.0 mmol), $[Ru(dmso)_4Cl_2]$ (484 mg, 1.0 mmol), and Et_3N (0.8 mL) in methanol (20 mL) was degassed with Ar and refluxed over 4 h. After the mixture cooled to room temperature, the mixture was filtered to get the residue, which was washed with cold methanol. **g** was obtained as dark brown solid, 189 mg (yied: 39%). ^1H NMR (500 MHz, d_6-dmso): δ = 8.68 (d, J = 10 Hz, 2 H), 8.19 (t, J =

Scheme 2. Selected Photocatalysts from Literature and This Work

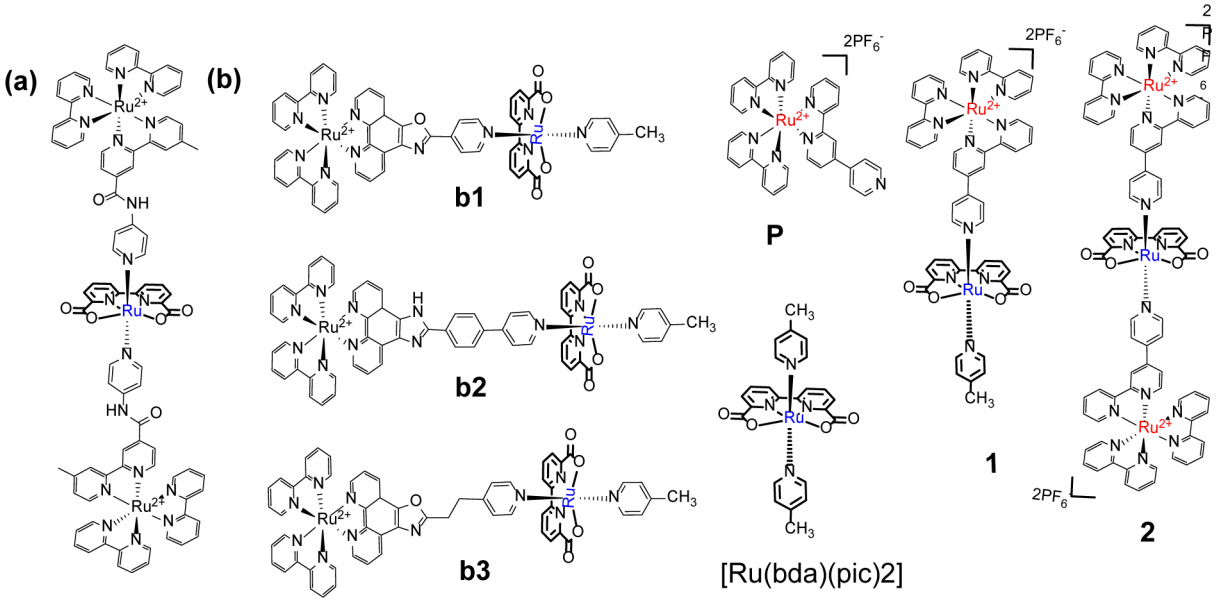

DOI: 10.1021/ic502915r
Inorg. Chem. 2015, 54, 2742−2751

10 Hz, 2 H), 8.08 (d, J = 10 Hz, 2 H), 3.2 (s, 6H). ES-MS$^+$: m/z^+ = 500.96 (M + H$^+$). Calcd: 500.9723.

*[Ru(bda)(dmso)4-picoline] (**h**).* A mixture of 4-picoline (30 mg, 0.32 mmol) and [Ru(bda)(dmso)$_2$] (**g**) (150 mg, 0.3 mmol) in methanol was degassed with Ar, and then stirred at room temperature for 24 h. The reaction mixture was dried in vacuum, and after purification by column chromatography on silica gel using dichloromethane/methanol (3:1) as eluent, a brown solid was obtained, 55 mg (yield: 30%). ^{1}H NMR (500 MHz, CD_3OD): δ = 8.56 (m, 2 H), 8.01 (m, 4 H), 7.73 (d, J = 10 Hz, 2 H), 7.16 (d, J = 10 Hz, 2 H), 2.87 (s, 6 H), 2.29 (s, 3 H). ES-MS$^+$: m/z^+ = 516.01 (M + H$^+$). Calcd: 516.0162.

*Ru Photosensitizer (**P**).* A solution of the bpyp (**e**) (233 mg, 0.1 mmol) and 484 mg (0.1 mmol) of *cis*-[Ru(bpy)$_2$Cl$_2$] in a 50 mL mixture of EtOH/H$_2$O (3:1) was heated at reflux in the dark under an argon atmosphere overnight. The solvents were removed by rotary evaporation, and the crude dark red residue was dissolved in a minimum amount of a CH_3CN/water 3 N KNO_3 (9:1) mixture and loaded on a silica gel column. Elution with pure CH_3CN removed the unreacted [Ru(bpy)$_2$Cl$_2$]. More rinsing with a CH_3CN/aq 3 N KNO_3 (9:1) mixture afforded the desired ester complex with NO_3^- as counteranion. The pure fractions of the target product were collected and dried under vacuum. After extraction of the resulting aqueous solution with dichloromethane twice, 0.8 g of KPF_6 was added to precipitate the final product. The organic phase was dried over $MgSO_4$ and the solvent removed to give the product with PF_6^- anions, 750 mg (yield 80%). ^{1}H NMR (500 MHz, CD_3OD): δ = 9.04 (d, J = 5 Hz, 1 H), 8.94 (d, J = 10 Hz, 1 H), 8.80 (d, J = 10 Hz, 2 H), 8.73 (d, J = 10 Hz, 4 H), 8.18 (m, 5 H), 7.97 (m, 4 H), 7.86 (m, 5 H), 7.58 (m, 5 H). ES-MS$^+$: m/z^+ = 323.56 (M^{2+}). Calcd: 323.5680.

*Complex **1**.* A mixture of (50 mg, 0.1 mmol) [Ru(bda)(dmso)4-picoline] (**h**) and Ru photosensitizer P (100 mg, 0.11 mmol) in methanol was degassed with Ar, and then stirred at 75 °C for 24 h. This was then dried in vacuum, and afterwards was purified by column chromatography on silica gel using aq 3 N KNO_3/CH_3CN (1:30) as eluent. Then the product solution was dried by vacuum, and the residue was dissolved in CH_3CN to remove the undissolved KNO_3. The CH_3CN solution was dried; after that the material was dissolved in water, the counterion was changed to PF_6^-, and a red solid was obtained, 55 mg (yield: 30%). ^{1}H NMR (500 MHz, CD_3OD): δ = 8.81 (s, 1 H), 8.71 (d, J = 10 Hz, 1 H), 8.58 (m, 6H), 8.02 (m, 6 H), 7.95 (m, 3 H), 7.85 (t, J = 10 Hz, 2 H), 7.70 (m, 6 H), 7.61 (m, 5 H), 7.37 (m, 5 H), 6.99 (d, J = 10 Hz, 2 H), 2.19 (s, 3H). ES-MS$^+$: m/z^+ = 542.0648 (M^{2+}). Calcd: 542.0668. Anal. Calcd ($C_{53}H_{40}F_{12}N_{10}O_4P_2Ru_2\cdot 1.9CH_3CN$): C, 47.02; H, 3.17; N, 11.49. Found: C, 47.38; H, 2.96; N, 11.82.

*Complex **2**.* A mixture of [Ru(II)L(dmso)$_2$] (**g**) (45 mg, 0.1 mmol) and Ru photosensitizer P (200 mg, 0.22 mmol) in methanol was degassed with Ar, and then stirred at 75 °C for 24 h. This was then dried in vacuum, and purified after by column chromatography on silica gel using aq 3 N KNO_3/CH_3CN (1:30) as eluent. Then, the product solution was dried by vacuum, and the residue was dissolved in CH_3CN to remove the undissolved KNO_3. The CH_3CN solution was dried, and after that dissolved in water. The counterion was changed to PF_6^-, a red solid was obtained, 65 mg (yield: 28%). ^{1}H NMR (500 MHz, CD_3OD): δ = 8.89 (s, 2 H), 8.79 (d, J = 10 Hz, 2 H), 8.66 (m, 10 H), 8.06 (m, 16 H), 7.97 (t, J = 10 Hz, 2 H), 7.83 (d, J = 5 Hz, 4 H), 7.80 (d, J = 5 Hz, 2 H), 7.77 (t, J = 5 Hz, 6 H), 7.73 (d, J = 5 Hz, 4 H), 7.68 (d, J = 5 Hz, 2 H), 7.45 (m, 10 H). ES-MS$^+$: m/z^+ = 409.3039 (M^{4+}). Calcd: 409.3034. Anal. Calcd ($C_{82}H_{60}F_{24}N_{16}O_4P_4Ru_3\cdot 0.8CH_3CN$): C, 44.64; H, 2.80; N, 10.46. Found: C, 44.38; H, 2.97; N, 11.78.

Electrochemistry. Differential pulse voltammetry and cyclic voltammetry were performed in phosphate buffer (pH 7) solution, measured by an Autolab potentiostat with a GPES electrochemical interface (EcoChemie), using glass carbon (diameter 3 mm) as the working electrode, an Ag/AgCl electrode (3 M KCl aqueous solution) as the reference electrode, and a platinum column as the counter electrode. Potentials are versus NHE by using [Ru(bpy)$_3$Cl$_2$] as a reference with $E(Ru^{2+/3+})$ = 1.26 V.

Water Oxidation Driven by Visible Light. A 100 mL round-bottomed flask was charged with 10 mL of ∼pH 7 buffer solutions (50 mM), 10% of CH_3CN, suitable concentrations of catalysts, and sacrificial electron acceptor $Na_2S_2O_8$. The flask was maintained in a circulating water cooling system and connected to the gas chromatograph via a 1/16 in. gas sampling tube; the reaction mixture was degassed with helium for 20 min before being illuminated with visible light. The photochemical oxygen evolution was investigated under irradiation with a 500 W xenon lamp equipped with a 400 nm cutoff filter to remove UV and a water jacket to maintain the reaction temperature around 20 °C, respectively. The irradiation intensity is ∼250 mW/cm^2, and the generated O_2 was measured by a 3000A Micro-GC.

Quantum Yield Measurement. A 10 mL portion of pH 7.0 boric acid buffer (20 mM) solution containing 10% of acetonitrile, catalyst (400 μM), and sacrificial electron acceptor $Na_2S_2O_8$ (40 mM) was thoroughly degassed with helium before irradiation. The volume of evolved O_2 after 10 min of irradiation was measured by GC. A 450 blue light was used as the light source, with a Galilean beam expander to control the strength of irradiance. The incident radiant power was measured by a calibrated laser power meter (Ophir Optronics Nova II) and a thermopile sensor (Ophir Optronics 3A-P-FS).

Steady State Absorption Measurements. A Cary 50 Bio UV−vis spectrophotometer (Varian) and a PerkinElmer Lambda 750 UV−vis spectrophotometer were used for steady state UV−vis measurements.

Steady State Emission Measurements. The instrument used was a Fluorolog 3-222 emission spectrophotometer (Horiba Jobin Yvon) together with the FluorEssence software. All the emission spectra were measured on samples at right angle with respect to the excitation light.

Flash Quench Measurements. Two nanosecond flash photolysis setups were used for the nanosecond transient measurements. The first was a frequency tripled Q-switched Nd:YAG laser from Quantel (BrilliantB) which was employed to obtain 355 nm pump light with a FWHM of 10 ns. The pump wavelength was then obtained by passing the third harmonic laser light through an OPO crystal (OPOTEK). The detection system was from Applied Photophysics, and probing was performed with a pulsed 150 W xenon arc lamp and signal detection by a 5-stage PMT detector. The detector was connected to a 600 MHz 10 GSa/s Agilent Technologies infiniium oscilloscope. All measurements were performed at a right angle with respect to the pump light.

The second laser system was a frequency tripled Q-switched Nd:YAG laser (Quanta-Ray ProSeries, Spectra-Physics) employed to obtain 355 nm pump light with a FWHM of 10 ns. The pump wavelength was then obtained by passing the third harmonic laser light through an OPO crystal. Probing was performed with a pulsed XBO 450 W xenon arc lamp (Osram), and signal detection by the iStar CCD camera (Andor Technology) of an LP920-S laser flash photolysis spectrometer setup (Edinburgh Instruments) was performed at a right angle with respect to the pump light. Transient signal detection was performed with LP920-K PMT detector which was connected to a Tektronix TDS 3052 500 MHz 5 GS/s oscilloscope. Transient absorption data was acquired using the L900 software (Edinburgh Instruments) and processed using Origin 9 software. A fluorescence quartz cell cuvette (Starna) with a 10 mm path length was used for measurements.

Time-Correlated Single-Photon Counting (TCSPC) Measurements.[40] A 20 MHz (tunable) picosecond diode laser (Edinburgh Instruments) at 470 nm (90 ps pulses) was used as excitation source. The laser's pulse energy was attenuated to the desired count rate of ca. 1% or less of the excitation frequency.

A cooled (ca. −40 °C) Hamamatsu Microchannel plate (MCP)-photomultiplier R3809U-51 was used for detection of single photons, and the signal passed through a discriminator (Ortec 9307) and into a TAC (Ortec 566). The electrical trigger signal from the laser was also passed through a discriminator (Tennelec TC454) and on to the TAC (Ortec 566). The TAC output was read by a DAQ-1 MCA computer

DOI: 10.1021/ic502915r
Inorg. Chem. 2015, 54, 2742−2751

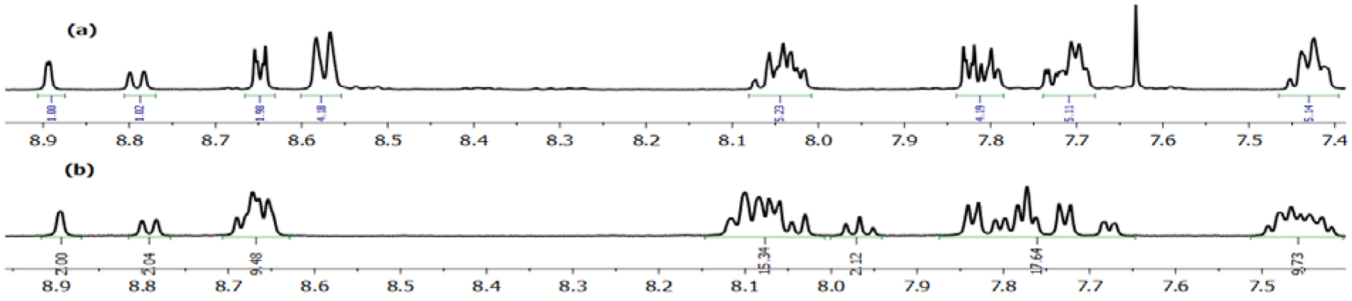

Figure 1. ^{1}H NMR spectra of complexes **P** (a) and **2** (b).

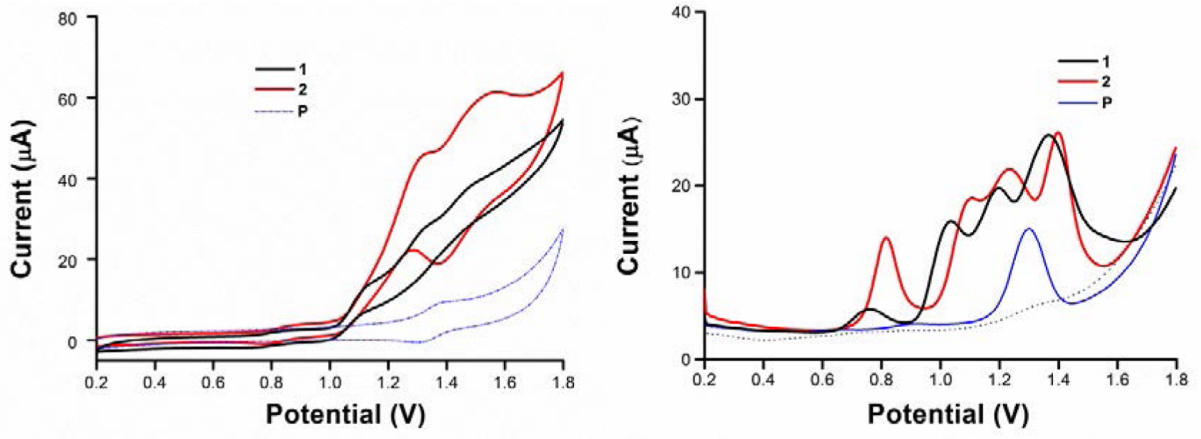

Figure 2. CVs (left) and DPVs (right) of complexes **1**, **2**, and **P** (potentials are reported vs NHE). Conditions: glassy carbon working electrode; 0.4 mM samples in 3.3 mL boric acid buffer solution (pH 7.0, containing 10% acetonitrile); a scan rate of 100 mV s^{-1} for CVs; and a step potential of 5 mV and amplitude of 50 mV for DPV.

card collected with Horiba Jobin Yvon DataStation 2.3. Measurements where performed under magic angle polarization.

Pump−Probe Measurements.[41] Time resolved pump−probe measurements were performed using a laser system consisting of a 1 kHz Ti:sapphire amplifier (Legend-HECryo,Coherent) pumped by a frequency doubled Q-switched Nd:YLF laser (Evolution-30, Coherent) and seeded by a mode-locked Ti:sapphire oscillator (Vitesse-800, Coherent). The output is 800 nm pulses with a temporal width of about 100 fs, while the instrument response time is about 150 fs. The beam is split into a pump and a probe beam. The pump light is directed to an optical parametric amplifier (TOPAS, Light Conversion) and converted to 435 nm light. The pump light then passes through a mechanical chopper which blocks every second pulse and is later focused in the sample cell. Before the sample cell, part of the pump light is led to a diode to reject extreme pulses (<10%). The probe light is directed to a delay mirror and thereafter focused on a vertically moving CaF_2 crystal for white light generation. The light is then split in two parts to be used as probe and reference. The probe light is first focused on the sample and overlapped with the chopped pump. Both probe and reference are divided spatially on an optical diffraction grating and further detected on a double diode array to give I/I_0 of every pair of pulses (pump on and pump off). The polarization of the pump pulse for all experiments was set to magic angle, 54.7°, with respect to the probe pulse. The step length in delay time varied between the measurements. Data analysis was performed with Origin. All spectra are corrected for chirp in the white light probe; time zero is set at maximum pump−probe temporal overlap. The region around pump wavelength is removed due to scatter of pump light.

RESULTS AND DISCUSSION

Synthesis and Structure. For the synthesis, $[Ru(bpy)_2(bpyp)]^{2+}$ (**P**) containing a free pyridine for coordination with the Ru-bda core was prepared through Suzuki coupling reaction (Supporting Information Scheme S1). Complexation of **P** with [Ru(bda)(dmso)(picoline)] gave the desired complex **1** in 32% yield. Reaction of **P** with another Ru-bda complex $[Ru(bda)(dmso)_2]$ generated complex **2** in 38% isolated yield (Scheme 2). Both complexes **1** and **2** were fully characterized by ^{1}H/^{13}C NMR and high resolution MS (Supporting Information Figure S1−3). The ^{1}H NMR spectra of **1** (Supporting Information Figure S1) and **2** (Figure 1) in CD_3OD are in good agreement with the structures of the all-in-one assemblies, and characteristic signals of the $[Ru(bpy)_2(bpyp)]^{2+}$ moiety remained more or less the same after it coordinated with the Ru-bda core. As shown in Figure 1, the symmetric structure of complex **2** was indicated by the even number of proton signals at 8.89, 8.79, and 7.45 ppm assigned to the two photosensitizer moieties. With respect to the catalytic center, signal at 7.97 ppm can be clearly assigned to the bda^{2-} ligand. The MS spectra of both **1** and **2** also confirmed the right structures of the all-in-one assemblies according to the multiple charges in the whole molecules (Supporting Information Figure S3); MS signals at m/z = 542.0648 and 409.3039 are assigned to species of $[\mathbf{1} - 2PF_6^-]^{2+}$ and $[\mathbf{2} - 4PF_6^-]^{4+}$, respectively, and the major signals at m/z^+ = 323.56 and 792.00 are attributed by $[\mathbf{P}]^{2+}$ and $[\mathbf{P} + PF_6^-]^+$, respectively.

Electrochemical Properties. The electrochemical properties of complexes **1**, **2**, and **P** were investigated in the 50 mM boric acid buffer solutions (10% acetonitrile, pH = 7) using cyclic voltammetry (CV) and differential pulse voltammetry (DPV). Results are shown in Figure 2. The $Ru^{III/II}$ process of **P** was observed at 1.28 V versus NHE which is close to the value of $[Ru(bpy)_3]^{2+}$ (E = 1.26 V). The slight positive shift of E is caused by the electron withdrawing pyridine motif in complex

DOI: 10.1021/ic502915r
Inorg. Chem. 2015, 54, 2742−2751

P. Complex **2** shows four redox waves from 0.6 to 1.6 V. The DPV peak at $E_{1/2}$ = 1.41 V is assigned to the Ru^{II}/Ru^{III} process of the photosensitizer motifs and the rest to $Ru^{II} \rightarrow Ru^{III} \rightarrow Ru^{IV} \rightarrow Ru^{V}$ processes of the Ru-bda motif.[5,6] Detailed electrochemical data of these complexes are shown in Supporting Information Table S1. For both **1** and **2**, the $E_{1/2}$ of the photosensitizer Ru^{II}/Ru^{III} couple is more positive than the respective onset potential of catalyst for water oxidation, which thermodynamically allows these two all-in-one assemblies to catalyze water oxidation driven by light. It is worth noting that complex **2** exhibits a higher catalytic current (>1.10 V) than complex **1** does, indicating that **2** catalyzes electrochemical water oxidation more actively than **1**.

Photochemical Water Oxidation. UV−vis absorption spectra of all the complexes are shown in Figure 3. The visible

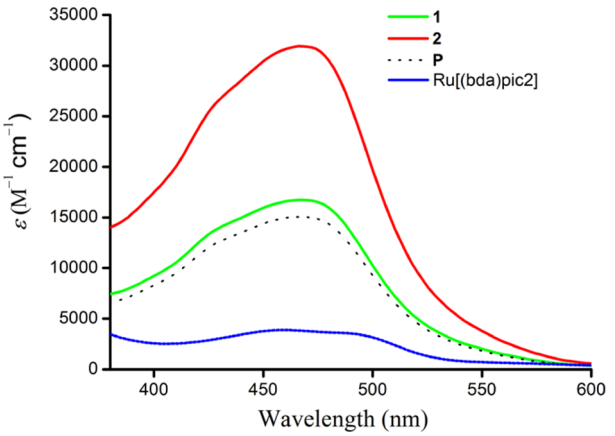

Figure 3. UV−vis spectra of complexes **1**, **2**, **P**, and [Ru(bda)(picoline)$_2$] in pH 7 buffer solution with 10% acetonitrile.

absorption band of [Ru(bda)(picoline)$_2$] is red-shifted and much weaker than for **P**. Thus, the sensitizer moiety absorbs the majority of visible light in **1** and **2**, as we expected.

Visible-light-driven water oxidation catalyzed by complexes **1** and **2** was carried out by using a two-component system consisting of a photocatalyst (**1** or **2**) and a sacrificial electron acceptor $Na_2S_2O_8$. In a typical experiment, photocatalyst and sodium persulfate were first dissolved in 10 mL of boric acid buffer (50 mM, pH 7.0 ± 0.2) solution containing 10% acetonitrile. The reaction mixture was maintained at 20 ± 2 °C by a water-jacket beaker and illuminated with a Xe-lamp with light intensity 250 mW/cm^2, using a λ >400 nm cutoff filter. The evolved oxygen in gas phase was analyzed with a 3000A Micro GC. The amount of oxygen evolution versus time is plotted as shown in Figure 4. Turnover numbers (TONs) of 78 and 209 were obtained for complexes **1** and **2**, respectively. Control experiments conducted under the same conditions using the mononuclear catalyst [Ru(bda)(picoline)$_2$] and the sensitizer $[Ru(bpy)_3]^{2+}$ show much less photocatalytic water oxidation activity (TON ∼17) that stops after a much shorter irradiation time. Without light irradiation of the solutions there is no detectable oxygen evolution for either of the systems. When oxygen evolution ceased in the experiments with **1** and **2**, the pH of the reaction solution had dropped dramatically, from 7.00 to 2.08 in the case of **2**. After neutralization of the buffer solution to the original pH value, it is noteworthy that the reaction system was able to restore ≈75% of its catalytic activity (Supporting Information Figure S4). Both catalysts **1** and **2** show much higher TONs than our previously published

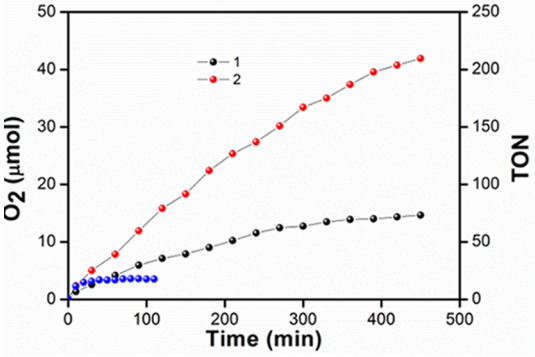

Figure 4. Photocatalytic oxygen evolution by the complexes **1** (black) and **2** (red) (20 μM) and $Na_2S_2O_8$ (20 mM) in pH 7 buffer solution. Control experiment (blue): oxygen produced by [Ru(bda)(picoline)$_2$] (20 μM) and $[Ru(bpy)_3(PF_6)_2]$ (40 μM) under the same condition.

photocatalyst, in which the amide bond was chosen as a linker between photosensitizer and catalyst.[34]

With complex **2** as an example, the kinetic measurement was conducted under the catalytic conditions. Using Ce(IV) as oxidant, we have previously demonstrated that the rate of water oxidation is second order in [Ru(bda)(picoline)$_2$].[6] As shown in Supporting Information Figure S6, second-order kinetics were observed also for **1** and **2** with Ce(IV) as oxidant. However, for light-driven water oxidation, we instead observed an apparent first-order dependence of the O_2 evolution rate on complex **2**. With a rate constant k_{O2} = 3.9 L min^{-1} for complex **2**, a linear (R^2 = 0.989) relationship is maintained. The first-order kinetics with respect to complex **2** can be explained by the fact that the photochemical reaction is not limited by the intrinsic reaction steps of the catalyst, but by the rate of light absorption. Under the experimental conditions, each sensitizer is excited about once per second, while the catalyst is capable of much higher TOFs. Only in cases where light levels are very high, catalyst TOFs are very low, or when the amount of catalyst is very small will the catalyst TOF be limiting. Otherwise, the observed rate of a typical photochemical water oxidation reaction with molecular units is therefore given by the rate of light absorption times the quantum yield for O_2 formation. The latter is in turn a product of the yields for the individual productive reaction steps: charge separation, oxidation of the catalyst, and completion of the catalytic cycle. Thus, the observed rates of photochemical oxygen evolution are typically not limited by the intrinsic steps of the catalyst. Consequently, the apparent change in reaction order with respect to the catalyst between the Ce(IV)- and light-induced conditions does not imply a change of the mechanism for O−O bond formation.

The quantum yield of photon-to-oxygen generation (eq 1) was determined using monochromatic light at 473 nm (90 mW/cm^2) in the initial phase of the reaction when the O_2 evolution rate was highest.

$$\Phi_{O2} = \frac{2n_{O2}}{n_{h\nu}} \quad (1)$$

$$n_p = \frac{(1-\rho)It\lambda}{N_A hc} \quad (2)$$

Note that ideally only two photons need to be absorbed to generate one O_2 molecule, because in addition to one oxidized

DOI: 10.1021/ic502915r
Inorg. Chem. 2015, 54, 2742−2751

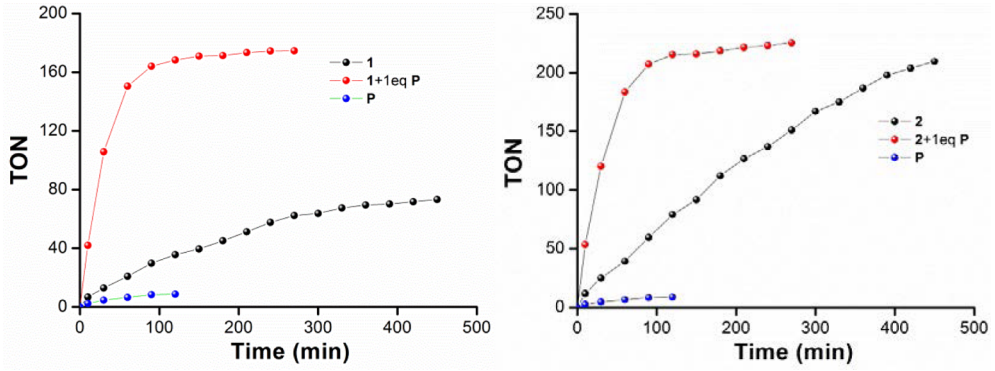

Figure 5. Oxygen evolution as a function of illumination time under the catalytic conditions. Left: both **1** and **P** (20 μM) (red); only **1**(20 μM) (black); only **P** (20 μM) (blue). Right: same measurement using **2**.

sensitizer (Ru^{III}), a second oxidizing equivalent $SO_4^{\bullet-}$ is generated:[17,30]

$$\mathbf{P} + h\nu \rightarrow \mathbf{P}^* \quad (3a)$$

$$S_2O_8^{2-} + \mathbf{P}^* \rightarrow SO_4^{2-} + SO_4^{\bullet-} + \mathbf{P}^+ \quad (3b)$$

$$SO_4^{\bullet-} + \mathbf{P} \rightarrow SO_4^{2-} + \mathbf{P}^+ \quad (3c)$$

Equation 2 was used to determine the moles of photons absorbed (n_p) where I is the irradiation power, λ is the light wavelength, t is the irradiation time, h is the Planck constant, N_A is the Avogadro constant, c is light speed, and ρ is the reflectance of the air/reaction vessel interface (6%). Φ_{O2} = 6.6% and 8.5% were measured for system **1**-$S_2O_8^{2-}$ and **2**-$S_2O_8^{2-}$, and 90% and 92% of the light was absorbed, respectively. When **P** and [Ru(bda)(picoline)$_2$] are in solution, Φ_{O2} = 34% (100% of the light was absorbed). Note that this value corresponds to the very first data points in the white-light irradiation experiments (250 mW/cm^2) of Figure 5. Thus, while the maximum TON is small for the three component system, the initial rate is much higher than that for the linked photocatalysts. This observation is discussed below.

In our previous work, the dissociation of photosensitizer motifs has been proposed as the major decomposition pathway for the photocatalyst.[34] Therefore, in the present study, 1 equiv of free photosensitizer **P** was added into the reaction mixture in order to inhibit the dissociation of photosensitizer motifs from photocatalysts **1** and **2**. The total efficiency of the water oxidation increased dramatically for both catalyst **1** and **2** (Figure 5). The initial reaction rates increased more than 2-fold. At the first glance, we believed that addition of complex **P** indeed ensured full binding of the catalyst units. However, when [Ru(bpy)$_3$]$^{2+}$, with no free coordinating pyridine, was used instead of **P** (Supporting Information Figure S8), a similar enhancement on the activity was observed. We could also show that a corresponding addition of the free ligand 4-picoline has essentially no effect on the catalytic activity (Supporting Information Figure S8). Thereby, the remarkable increase of water oxidation efficiency after adding free photosensitizer is not because of prevention of photosensitizer dissociation.

Spectroscopic Measurements. In order to better understand the photochemical reactions and the origin of this activity enhancement, kinetic measurements regarding **1**, **2**, **P**, and [Ru(bda)(picoline)$_2$] were conducted using photoemission spectroscopy as well as femtosecond and nanosecond transient absorption spectroscopy. Laser excitation of **P** (λ = 470 nm, FWHM = 10 ns, 10 mJ) gave a transient absorption spectrum that is typical for a metal-to-ligand charge transfer (MLCT) triplet excited state in [Ru(bpy)$_3$]$^{2+}$ derivatives (Supporting Information Figure S20), which decayed with a lifetime of 780 ns in N_2-purged solution. Excitation of [Ru(bda)(picoline)$_2$] with a femtosecond pulse (λ = 435 nm, fwhm = 200 fs) resulted in a very similar spectrum (Supporting Information Figure S22), with the only difference being a more narrow excited state absorption band in the red end than for **P**. Thus, we attribute this to the lowest ^{3}MLCT state of [Ru(bda)-(picoline)$_2$], presumably localized on the bda ligand, which decayed to the ground state with lifetime of 20 ps (Figure 6 and Supporting Information Figure S22).

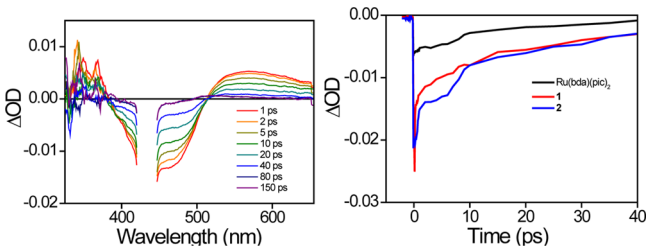

Figure 6. Left: transient absorption spectra of dyad **1** at different delay times after excitation at 435 nm (fwhm = 200 fs). Right: time traces at 470 nm from the corresponding experiments for **1**, **2**, and [Ru(bda)(picoline)$_2$]. Conditions: **1** in 9:1 aqueous 50 mM boric buffer/acetonitrile solution under nitrogen.

Femtosecond excitation of **1** or **2** resulted after 1 ps in a spectrum very similar to those for the excited states of the reference complexes, and that decayed with a lifetime of 20 ps (Figure 6 and Supporting Information Figure S21). A significant additional, ultrafast component ($\tau \approx 0.5$ ps) could be seen in the bleach recovery at 470 nm of **1** and **2**, that is not present in [Ru(bpy)$_3$]$^{2+}$[42,43] or [Ru(bda)(picoline)$_2$]. After 150 ps, however, the presence of a different species is clear from the spectra, with a band maximum around 510 nm that rises (τ = 20 ps). The spectrum is in excellent agreement with a reduced [Ru(bpy)$_3$]$^+$ sensitizer and ground state bleach of both units; i.e., we attribute this to the electron transfer products where the catalyst unit has been oxidized by the appended photosensitizer ($-\Delta G^\circ \approx 0.1$ eV; see Supporting Information). The magnitude of the 510 nm absorption at 150 ps is quite small compared to the initial MLCT features, however, showing that this is only a minor reaction with 5−10% yield (the extinction coefficients for the reduced [Ru(bpy)$_3$]$^+$ at 510 nm and the MLCT bleach at 450 nm are similar[44]). The 510 nm absorption signal decays

DOI: 10.1021/ic502915r
Inorg. Chem. 2015, 54, 2742−2751

on the microsecond time scale, but if persulfate is present it disappears much faster (Figure 7 and Supporting Information

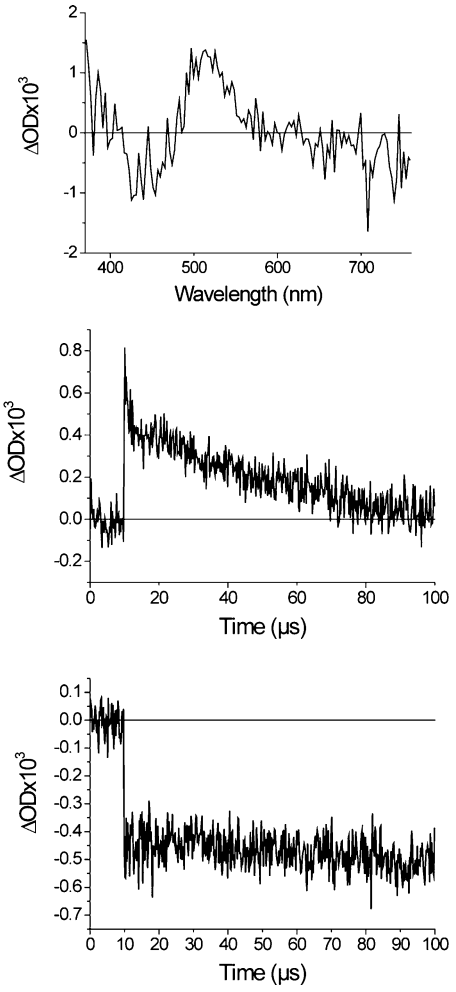

Figure 7. Transient absorption data of triad **2**. The top panel shows the spectrum at 200 ns after excitation. The middle and lower panels show, respectively, the transient absorption time traces at 510 nm without and with 20 mM persulfate. Conditions: **2** in 9:1 aqueous 50 mM boric buffer/acetonitrile under nitrogen; excited at 470 nm, fwhm = 10 ns, 15 mJ/pulse.

Figure S24), indicating rapid regeneration of the sensitizer by persulfate. The low electron transfer yield in Figure 6 (left) shows that excited state quenching occurs mainly via a different reaction, however. Electron transfer *to* the catalyst from the excited sensitizer unit can be excluded, as it is endergonic by ca. 0.5 eV (see Supporting Information). Instead, we propose that ultrafast energy transfer from the sensitizer to the catalyst unit occurs ($\tau \approx 0.5$ ps), and that the catalyst MLCT state then decays to the ground state with $\tau = 20$ ps just like in the reference [Ru(bda)(picoline)$_2$]. The driving force for the energy transfer step can be estimated to $-\Delta G^\circ \approx 0.30$ eV from the 77 K photoemission spectra of **P** and [Ru(bda)(picoline)$_2$] (Supporting Information Figure S23). The small fraction of electron transfer from the catalyst presumably occurs already in the ^{3}MLCT state of the sensitizer unit, in parallel to energy transfer, as electron transfer from excited [Ru(bda)(picoline)$_2$] is estimated to be endergonic by ca. 0.20 eV (see Supporting Information). A more detailed discussion of these processes and assignments can be found in the Supporting Information.

Photoemission spectra with excitation at 555 nm confirm that the sensitizer phosphorescence is strongly quenched in **1** and **2**, with relative quantum yields of 0.06 and 0.04, respectively, compared to **P** (Supporting Information Figure S14). Time resolved emission data at 620 nm (excitation at λ = 470 nm, fwhm = 10 ns, 10 mJ/pulse) showed a single exponential decay with a lifetime of 770 and 650 ns for **1** and **2**, respectively, similar to that of **P** (780 ns). In oxygenated solution (1 atm O_2) the lifetime drops to 210 ns due to oxygen quenching. Because of the ultrafast excited state quenching shown in the transient absorption experiments above (lifetime <20 ps), **1** and **2** are expected to give negligible contribution (<0.1%) to the emission intensity, while essentially all emission comes from a small fraction of unquenched sensitizer that presumably is not bound to a catalyst unit. Therefore, from a combination of time-resolved and steady state emission data, we estimate the amount of unbound sensitizer to be ca. 6% and 4%, respectively, for **1** and **2**. To investigate if the unquenched fraction is due to a dynamic coordination equilibrium of the sensitizer with the catalyst, a dyad solution was titrated with picoline that would compete for binding to the catalyst. This did not lead to any significant increase in emission even in the presence of 0.55 M picoline, showing that there is no dynamic equilibrium between dyad and the sensitizer (Supporting Information Figure S15).

Additional quenching studies of **P** with [Ru(bda)(picoline)$_2$] and with $Na_2S_2O_8$ yielded bimolecular rate constants for both processes. The rates for these processes were in turn used to predict the quantum yield of oxygen evolution in the three-component systems with separate sensitizer and catalyst

$$\Phi_{O_2} = \phi_{CE}\left(\frac{k_q}{k_q + k_{ex} + k_{en1}[O_2] + k_{en2}[\text{cat.}]}\right) \quad (4)$$

where Φ_{O_2} is the quantum yield of oxygen evolution, ϕ_{CE} is the cage escape yield in the quenching reaction with $S_2O_8^{2-}$ ($\phi_{CE} \approx 1$ in the present system), k_q is the electron transfer rate constant between **P** and 20 mM $Na_2S_2O_8$, k_{ex} is the excited state decay rate constant, k_{en1} is the rate constant for energy transfer between **P** and oxygen (1 atm), and k_{en2} is the rate constant for energy transfer between **P** and [Ru(bda)(picoline)$_2$]. The following values were used:

$$k_q = \frac{1}{90\text{ ns}},\ k_{ex} = \frac{1}{780\text{ ns}},\ k_{en1}[O_2] = \frac{1}{210\text{ ns}} - \frac{1}{780\text{ns}},\ k_{en2} = 2{*}10^9\ M^{-1}\,s^{-1},\ [\text{cat.}] = 20\ \mu M,\ \phi_{CE} = 1$$

The quantum yield of oxygen evolution calculated from eq 4 is 70%. This assumes that all the losses are due to competing pathways for excited state decay and that the oxidative equivalents generated (Ru(III) and $SO_4^{\bullet-}$) undergo no recombination or side reactions but are only used to advance the oxidation state of the catalyst and thus split water. This is about twice the experimental value (34%). This difference may be due to two factors: First, the $SO_4^{\bullet-}$ equivalents may be lost by other reactions than further oxidation of the catalyst or sensitizers. Second, the higher oxidation states of the catalyst that are formed may quench the excited sensitizer by nonproductive (oxidative) electron transfer or energy transfer. For the bimolecular reactions, however, this cannot be the

DOI: 10.1021/ic502915r
Inorg. Chem. 2015, 54, 2742−2751

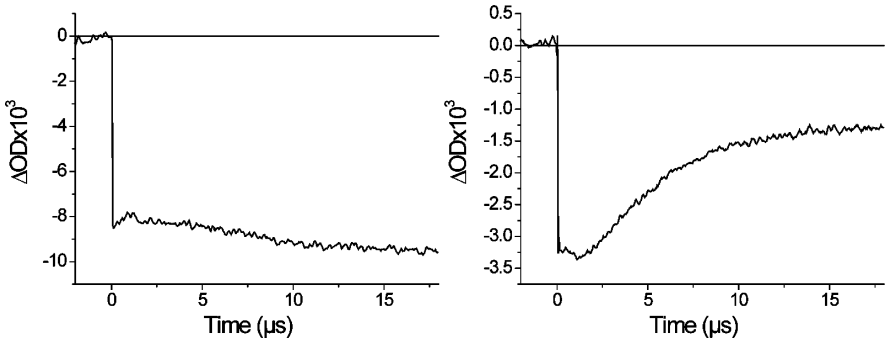

Figure 8. Transient absorption traces for **P** and persulfate at 450 nm showing the Ru(II) ground state bleach of the photooxidized sensitizer. Left: the initial bleach is followed by a further small bleach, possibly due to reaction of $SO_4^{\bullet-}$ radicals with ground state **P**. Right: bleach recovery in the presence of 0.13 mM [Ru(dba)(picoline)$_2$]. Conditions: 3.3 mM persulfate and 30 μM P in 9:1 aqueous 50 mM boric buffer:acetonitrile under nitrogen; excitation at 470 nm, fwhm = 10 ns, 13 mJ/pulse.

explanation as already quenching by the Ru(II) catalyst is near diffusion controlled.

Laser flash experiments of **P** with [Ru(bda)(picoline)$_2$] and $Na_2S_2O_8$ show that **P** is initially photo-oxidized by persulfate, but is rapidly regenerated by the catalyst (Figure 8). Both oxidized **P** and catalyst show a ground state bleach around 450 nm, but the extinction coefficient for the latter is smaller (cf. Figure 3 and Supporting Information Figure S10). This leads to the partial bleach recovery seen in Figure 8, right panel. From the kinetics and the concentration of catalyst we can estimate that the reaction is near-diffusion controlled ($\sim 1 \times 10^9$ M^{-1} s^{-1}).

Attempts were made to study the catalyst reactions in higher oxidation states by transient spectroscopy. Electron transfer from $[Ru(bda)(picoline)_2]^+$ to $\mathbf{P}^+$ is the next step in photocatalysis, and it is even believed that the catalytic cycle starts from $[Ru(bda)(picoline)_2]^+$ while [Ru(bda)(picoline)$_2$] is in fact a precatalyst. However, attempts at preparing the Ru(III) species $[Ru(bda)(picoline)_2]^+$ by air oxidation of [Ru(bda)(picoline)$_2$] at room temperature for ~15 min led to irreversible accumulation of a side product. This is a side product formed by the catalyst after oxidation over the time scale of ~1 h, with an absorption peak at 689 nm (Supporting Information Figures S16 and S17). The side product forms slowly enough to not be involved in the catalytic cycles, but unfortunately too rapidly to allow for transient spectroscopy studies when the catalyst are in the higher oxidation states. Laser flash experiments of the oxidized solution with sensitizer and $S_2O_8^{2-}$ show that the main result is electron transfer to the side product (Supporting Information Figures S18 and S19), which precluded any conclusions regarding photosensitized reactions of $[Ru(bda)(picoline)_2]^+$.

For the linked photocatalyst systems **1** and **2** instead, the much lower Φ_{O2} values than that for the three-component system can be explained by the rapid, mainly unproductive quenching by intramolecular energy transfer between the sensitizer moiety and the catalyst moiety within dyad **1** and triad **2**. It is also clear from the experiments with **1**, **2**, and additional **P** (Figure 5, Supporting Information Figures S7 and S8) that some O_2 is generated via excitation of the small fraction of free sensitizer detected in the photoemission experiment. This cannot, however, explain the entire O_2 yield: First, the free sensitizer fraction is larger for **1** (6%) than for **2** (4%), based on the photoemission measurements, whereas the observed Φ_{O2} in oxygen evolution experiments is smaller for **1** (6.6%, vs 8.5% for **2**). Second, for the three-component system where all sensitizer is unbound (i.e., 25 times more free sensitizer than in **2**) Φ_{O2} = 34%, which is only 4 times larger than the yield for **2**. We therefore conclude that also the linked sensitizer in **1** and **2** is very active in O_2 generation. The fraction (5−10%) of charge separated state observed in the femtosecond transient absorption experiments (see Figures 6 and 7, Supporting Information Figures S21 and S24), that is seen to react with $S_2O_8^{2-}$ (see Figure 7), advances **1** and **2** to the Ru(III) state of the catalyst. Direct information on higher oxidation states of the catalyst that correspond to the later steps in the photocatalytic cycle would be highly desirable, but were unfortunately precluded in the present case by the instability of the Ru(III) state toward formation of a side product on preparative time scales (see above). Nevertheless, because the observed Φ_{O2} is much smaller than 100% we can conclude that also higher oxidation states of the catalyst units in **1** and **2** quench the sensitizer by partly unproductive mechanisms.

To conclude this discussion, we turn to a discussion of two important effects, shown in this work, of linking the sensitizer and catalyst. The first is the increased photostability of the linked systems **1** and **2** in O_2 evolution experiments, and the second is the rapid, nonproductive energy transfer quenching of the sensitizer excited state by the catalyst. Regarding the first effect, the three-component system shows very poor photostability. As we have shown previously,[45] this is mainly because of sensitizer degradation (although some catalyst decomposition is also observed); when more sensitizer is added after O_2 evolution has stopped, the photocatalysis recommences. However, in the present study, addition of only 1 equiv (Figure 5) or 0.25 equiv (Supporting Information Figure S7) of **P** to a solution of **2** leads to much higher rate than with only **2** until the reaction stops because of the low pH in solution. If the free **P** would have been as photosensitive as in the three-component experiments, the effect of the addition would have been very short-lived. The photosensitivity of the free **P** is mainly due to its instability in the oxidized state in neutral aqueous solution. While electron transfer from the Ru(II)-state of the catalyst to $\mathbf{P}^+$ is already diffusion controlled, further catalyst oxidation has a lower driving force and is proton-coupled[4−6] and is therefore expected to be much slower. Therefore, the sensitizer units of **1** and **2** may act as electron transfer relays between the catalyst and free $\mathbf{P}^+$ in the later stages of the oxidation cycle to protect the free **P**, similar to the relay effect reported in related systems.[42] We note that the second step of the relay, intramolecular oxidation, can still be

DOI: 10.1021/ic502915r
Inorg. Chem. 2015, 54, 2742−2751

rapid in the higher oxidation states compared to the bimolecular reaction with 20 μM catalyst, which may explain the stabilization of the sensitizer units in **1** and **2**. So, in conclusion, linking of the catalyst to the sensitizer allows for a more rapid electron transfer to both the appended sensitizer and to the free **P**, compared to the case of a completely bimolecular system, so that sensitizer regeneration may compete better with its decomposition.

The second effect we discuss here is the rapid, nonproductive quenching of the excited sensitizer by the linked catalyst, which is similar to what has been observed before for other catalysts or catalyst models linked to photosensitizers. Transition-metal complexes have in general low-lying excited states, even if the direct transition is not seen in the absorption spectrum. These can quench by exchange energy transfer. In addition, as soon as the catalyst is oxidized in one step, quenching may occur by reverse electron transfer,[46] reducing the catalyst again. These unproductive reactions must be kinetically outcompeted by the productive ones, in order to obtain efficient photocatalytic systems. The unproductive reactions may be slower, for example, by localizing the sensitizer MLCT state on the ligands remote from the catalyst. A reduction in quenching rate by up to a factor of 1000 has been demonstrated with this strategy.[47,48] Also, the productive, oxidative quenching of the sensitizer by an acceptor can be made faster, by, e.g., linking the sensitizer to TiO_2 surfaces for ultrafast electron injection.[48] Both strategies are directly applicable to the present systems, by substituting the remote sensitizer ligands with electron-withdrawing groups that also anchor to semiconductors. This points to the use of such modified systems in dye-sensitized solar fuels devices with molecular catalysts, which is a field of strong current activity.[49,50]

CONCLUSIONS

We have demonstrated two stable photocatalyst assemblies **1** and **2** consisting of water oxidation catalyst and photosensitizer linked via a single C−C bond. Assembly **2** gives a higher rate of O_2 evolution and is more stable than **1**. The combined information from photocatalytic experiments and time-resolved spectroscopy underlines both the pros and the cons with a covalently linked sensitizer-catalyst system. The linked system allows for a faster sensitizer regeneration and oxidation of the catalyst, which kinetically enhances the sensitizer photostability. In addition the sensitizer moieties in the assemblies appear to act as electron transfer relays between the catalyst and free $\mathbf{P}^+$, which also prevents the free **P** from decomposition. Thus, linking of the catalyst to the sensitizer allows the rapid electron transfer to both the appended and free sensitizer, resulting in a better photostability. On the other hand, the catalyst in close proximity introduces competing excited state quenching pathways leading to a strong reduction in yield. These problems can be overcome by a suitable design of the sensitizer to decrease the rates of these competing reactions. Moreover, as electron injection into TiO_2 from many excited sensitizers is known to occur on the subpicosecond scale, the unwanted reactions may be outcompeted by immobilizing the photocatalyst assemblies onto a TiO_2 film. This can be used to build a highly efficient photoanode, which motivates further study to get deeper insights into the kinetic and mechanistic factors that govern the reaction efficiency of such a system.

ASSOCIATED CONTENT

Supporting Information

Experimental details containing the synthesis route; NMR, MS, and UV−vis spectra; kinetics and quantum yield measurements details. This material is available free of charge via the Internet at http://pubs.acs.org.

AUTHOR INFORMATION

Corresponding Author

*E-mail: Leif.Hammarstrom@kemi.uu.se.

Author Contributions

$^{\perp}$L.W. and M.M. contributed equally to this work equally.

Notes

The authors declare no competing financial interest.

ACKNOWLEDGMENTS

We thank the Swedish Research Council, Knut & Alice Wallenberg Foundation, the Swedish Energy Agency, China Scholarship Council (CSC), National Natural Science Foundation of China (21120102036), and the National Basic Research Program of China (2014CB239402) for financial support of this work.

REFERENCES

(1) Meyer, T. J. *Nature* **2008**, *451*, 778.
(2) Concepcion, J. J.; Jurss, J. W.; Brennaman, M. K.; Hoertz, P. G.; Patrocinio, A. O. v. T.; Murakami Iha, N. Y.; Templeton, J. L.; Meyer, T. J. *Acc. Chem. Res.* **2009**, *42*, 1954.
(3) Concepcion, J. J.; Tsai, M.-K.; Muckerman, J. T.; Meyer, T. J. *J. Am. Chem. Soc.* **2010**, *132*, 1545.
(4) Duan, L.; Araujo, C. M.; Ahlquist, M. S. G.; Sun, L. *Proc. Natl. Acad.Sci. U.S.A.* **2012**, *109*, 15584.
(5) Duan, L.; Bozoglian, F.; Mandal, S.; Stewart, B.; Privalov, T.; Llobet, A.; Sun, L. *Nat. Chem.* **2012**, *4*, 418.
(6) Duan, L.; Fischer, A.; Xu, Y.; Sun, L. *J. Am. Chem. Soc.* **2009**, *131*, 10397.
(7) Gersten, S. W.; Samuels, G. J.; Meyer, T. J. *J. Am. Chem. Soc.* **1982**, *104*, 4029.
(8) Wang, L.; Duan, L.; Stewart, B.; Pu, M.; Liu, J.; Privalov, T.; Sun, L. *J. Am. Chem. Soc.* **2012**, *134*, 18868.
(9) Wasylenko, D. J.; Ganesamoorthy, C.; Henderson, M. A.; Koivisto, B. D.; Osthoff, H. D.; Berlinguette, C. P. *J. Am. Chem. Soc.* **2010**, *132*, 16094.
(10) Zong, R.; Thummel, R. P. *J. Am. Chem. Soc.* **2005**, *127*, 12802.
(11) Romain, S.; Bozoglian, F.; Sala, X.; Llobet, A. *J. Am. Chem. Soc.* **2009**, *131*, 2768.
(12) Wang, L.; Duan, L.; Wang, Y.; Ahlquist, M. S. G.; Sun, L. *Chem. Commun.* **2014**, *50*, 12947.
(13) Blakemore, J. D.; Schley, N. D.; Balcells, D.; Hull, J. F.; Olack, G. W.; Incarvito, C. D.; Eisenstein, O.; Brudvig, G. W.; Crabtree, R. H. *J. Am. Chem. Soc.* **2010**, *132*, 16017.
(14) Hull, J. F.; Balcells, D.; Blakemore, J. D.; Incarvito, C. D.; Eisenstein, O.; Brudvig, G. W.; Crabtree, R. H. *J. Am. Chem. Soc.* **2009**, *131*, 8730.
(15) McDaniel, N. D.; Coughlin, F. J.; Tinker, L. L.; Bernhard, S. *J. Am. Chem. Soc.* **2008**, *130*, 210.
(16) Huang, Z.; Luo, Z.; Geletii, Y. V.; Vickers, J. W.; Yin, Q.; Wu, D.; Hou, Y.; Ding, Y.; Song, J.; Musaev, D. G.; Hill, C. L.; Lian, T. *J. Am. Chem. Soc.* **2011**, *133*, 2068.
(17) Berardi, S.; La Ganga, G.; Natali, M.; Bazzan, I.; Puntoriero, F.; Sartorel, A.; Scandola, F.; Campagna, S.; Bonchio, M. *J. Am. Chem. Soc.* **2012**, *134*, 11104.
(18) Dogutan, D. K.; McGuire, R.; Nocera, D. G. *J. Am. Chem. Soc.* **2011**, *133*, 9178.
(19) Leung, C.-F.; Ng, S.-M.; Ko, C.-C.; Man, W.-L.; Wu, J.; Chen, L.; Lau, T.-C. *Energy Environ. Sci.* **2012**, *5*, 7903.

DOI: 10.1021/ic502915r
Inorg. Chem. 2015, 54, 2742−2751

(20) McCool, N. S.; Robinson, D. M.; Sheats, J. E.; Dismukes, G. C. *J. Am. Chem. Soc.* **2011**, *133*, 11446.
(21) Wasylenko, D. J.; Ganesamoorthy, C.; Borau-Garcia, J.; Berlinguette, C. P. *Chem. Commun.* **2011**, *47*, 4249.
(22) Zhu, G.; Geletii, Y. V.; Kogerler, P.; Schilder, H.; Song, J.; Lense, S.; Zhao, C.; Hardcastle, K. I.; Musaev, D. G.; Hill, C. L. *Dalton Trans.* **2012**, *41*, 2084.
(23) Ellis, W. C.; McDaniel, N. D.; Bernhard, S.; Collins, T. J. *J. Am. Chem. Soc.* **2010**, *132*, 10990.
(24) Fillol, J. L.; Codola, Z.; Garcia-Bosch, I.; Gomez, L.; Pla, J. J.; Costas, M. *Nat. Chem.* **2011**, *3*, 807.
(25) Barnett, S. M.; Goldberg, K. I.; Mayer, J. M. *Nat. Chem.* **2012**, *4*, 498.
(26) Zhang, M.-T.; Chen, Z.; Kang, P.; Meyer, T. J. *J. Am. Chem. Soc.* **2013**, *135*, 2048.
(27) Geletii, Y. V.; Huang, Z.; Hou, Y.; Musaev, D. G.; Lian, T.; Hill, C. L. *J. Am. Chem. Soc.* **2009**, *131*, 7522.
(28) Vickers, J. W.; Lv, H.; Sumliner, J. M.; Zhu, G.; Luo, Z.; Musaev, D. G.; Geletii, Y. V.; Hill, C. L. *J. Am. Chem. Soc.* **2013**, *135*, 14110.
(29) Besson, C.; Huang, Z.; Geletii, Y. V.; Lense, S.; Hardcastle, K. I.; Musaev, D. G.; Lian, T.; Proust, A.; Hill, C. L. *Chem. Commun.* **2010**, *46*, 2784.
(30) Lewandowska-Andralojc, A.; Polyansky, D. E.; Zong, R.; Thummel, R. P.; Fujita, E. *Phys. Chem. Chem. Phys.* **2013**, *15*, 14058.
(31) Ashford, D. L.; Stewart, D. J.; Glasson, C. R.; Binstead, R. A.; Harrison, D. P.; Norris, M. R.; Concepcion, J. J.; Fang, Z.; Templeton, J. L.; Meyer, T. J. *Inorg. Chem.* **2012**, *51*, 6428.
(32) Kaveevivitchai, N.; Chitta, R.; Zong, R.; El Ojaimi, M.; Thummel, R. P. *J. Am. Chem. Soc.* **2012**, *134*, 10721.
(33) Vagnini, M. T.; Smeigh, A. L.; Blakemore, J. D.; Eaton, S. W.; Schley, N. D.; D'Souza, F.; Crabtree, R. H.; Brudvig, G. W.; Co, D. T.; Wasielewski, M. R. *Proc. Natl. Acad. Sci. U.S.A.* **2012**, *109*, 15651.
(34) Li, F.; Jiang, Y.; Zhang, B.; Huang, F.; Gao, Y.; Sun, L. *Angew. Chem., Int. Ed.* **2012**, *51*, 2417.
(35) Sun, L.; Gao, Y.; Yu, Z.; Ding, X.; Duan, L. *Faraday Discuss.* **2014**, DOI: 10.1039/C4FD00127C.
(36) Dulière, E.; Devillers, M.; Marchand-Brynaert, J. *Organometallics* **2003**, *22*, 804.
(37) Wenkert, D.; Woodward, R. B. *J. Org. Chem.* **1983**, *48*, 283.
(38) Mizuno, T.; Takeuchi, M.; Hamachi, I.; Nakashima, K.; Shinkai, S. *J. Chem. Soc., Perkin Trans. 2* **1998**, 2281.
(39) McClenaghan, N. D.; Barigelletti, F.; Maubert, B.; Campagna, S. *Chem. Commun.* **2002**, 602.
(40) El-Zohry, A.; Orthaber, A.; Zietz, B. *J. Phys. Chem. C* **2012**, *116*, 26144.
(41) Petersson, J.; Eklund, M.; Davidsson, J.; Hammarström, L. *J. Phys. Chem. B* **2010**, *114*, 14329.
(42) The ^{1}MLCT to ^{3}MLCT and vibrational relaxation gives much smaller changes of the ground state bleach maximum than observed here: refs 32 and 33.
(43) Wallin, S.; Davidsson, J.; Modin, J.; Hammarström, L. *J. Phys. Chem. A* **2005**, *109*, 4697.
(44) McCusker, J. K. *Acc. Chem. Res.* **2003**, *36*, 876.
(45) Wang, L.; Duan, L.; Tong, L.; Sun, L. *J. Catal.* **2013**, *306*, 129.
(46) Magnuson, A.; Anderlund, M.; Johansson, O.; Lindblad, P.; Lomoth, R.; Polivka, T.; Ott, S.; Stensjö, K.; Styring, S.; Sundström, V.; Hammarström, L. *Acc. Chem. Res.* **2009**, *42*, 1899.
(47) Abrahamsson, M. L. A.; Baudin, H. B.; Tran, A.; Philouze, C.; Berg, K. E.; Raymond-Johansson, M. K.; Sun, L.; Åkermark, B.; Styring, S.; Hammarström, L. *Inorg. Chem.* **2002**, *41*, 1534.
(48) Xu, Y.; Eilers, G.; Borgström, M.; Pan, J.; Abrahamsson, M.; Magnuson, A.; Lomoth, R.; Bergquist, J.; Polívka, T.; Sun, L.; Sundström, V.; Styring, S.; Hammarström, L.; Åkermark, B. *Chem.—Eur. J.* **2005**, *11*, 7305.
(49) Gao, Y.; Ding, X.; Liu, J.; Wang, L.; Lu, Z.; Li, L.; Sun, L. *J. Am. Chem. Soc.* **2013**, *135*, 4219.
(50) Youngblood, W. J.; Lee, S.-H. A.; Kobayashi, Y.; Hernandez-Pagan, E. A.; Hoertz, P. G.; Moore, T. A.; Moore, A. L.; Gust, D.; Mallouk, T. E. *J. Am. Chem. Soc.* **2009**, *131*, 926.

DOI: 10.1021/ic502915r
Inorg. Chem. 2015, 54, 2742−2751